STUDY OF 3+1D SPACETIME EVOLUTION OF GLASMA IN RELATIVISTIC HEAVY-ION COLLISION

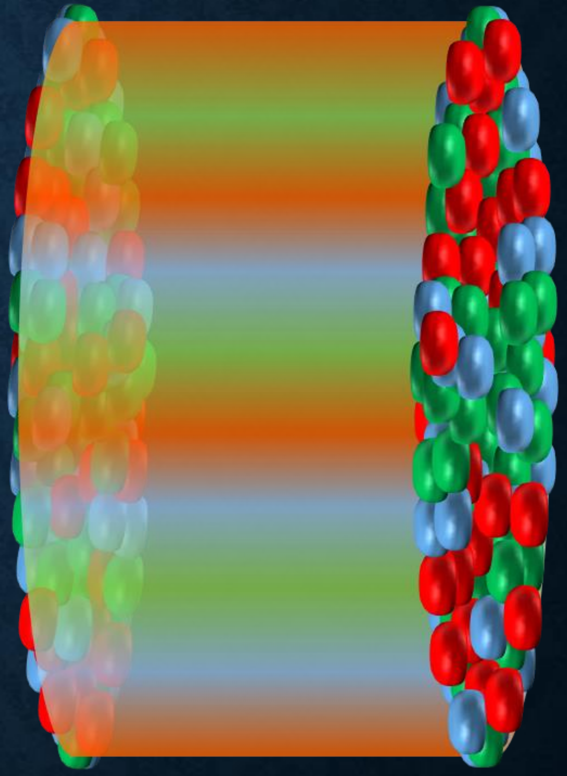

Hidefumi Matsuda (Zhejiang U.)

Collaborator: Xu-Guang Huang (Fudan U.)

Phys. Rev. D 108, 114008, (2023)
arXiv:2409.08742

West lake workshop on nuclear physics 2024, 18th October 2024

浙江大学 物理学院
SCHOOL OF PHYSICS
ZHEJIANG UNIVERSITY

Table of Contents

Table of Contents

Space-Time Evolution of HIC at RHIC and LHC

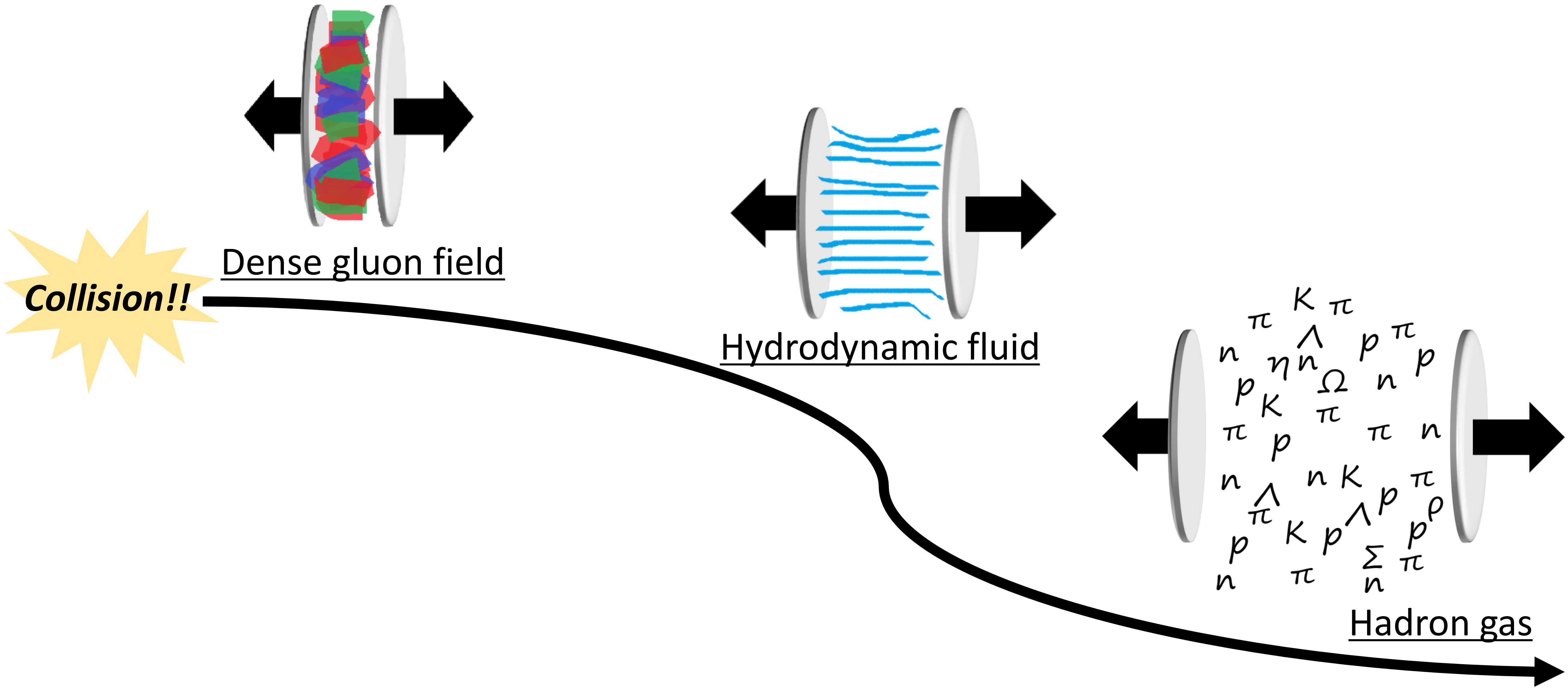

Phenomenological Analysis of the Evolution

1. Initial State Model

2. Relativistic Hydrodynamic Simulation

3. Cooper-Frye Formula

4. Hadron Transport Model

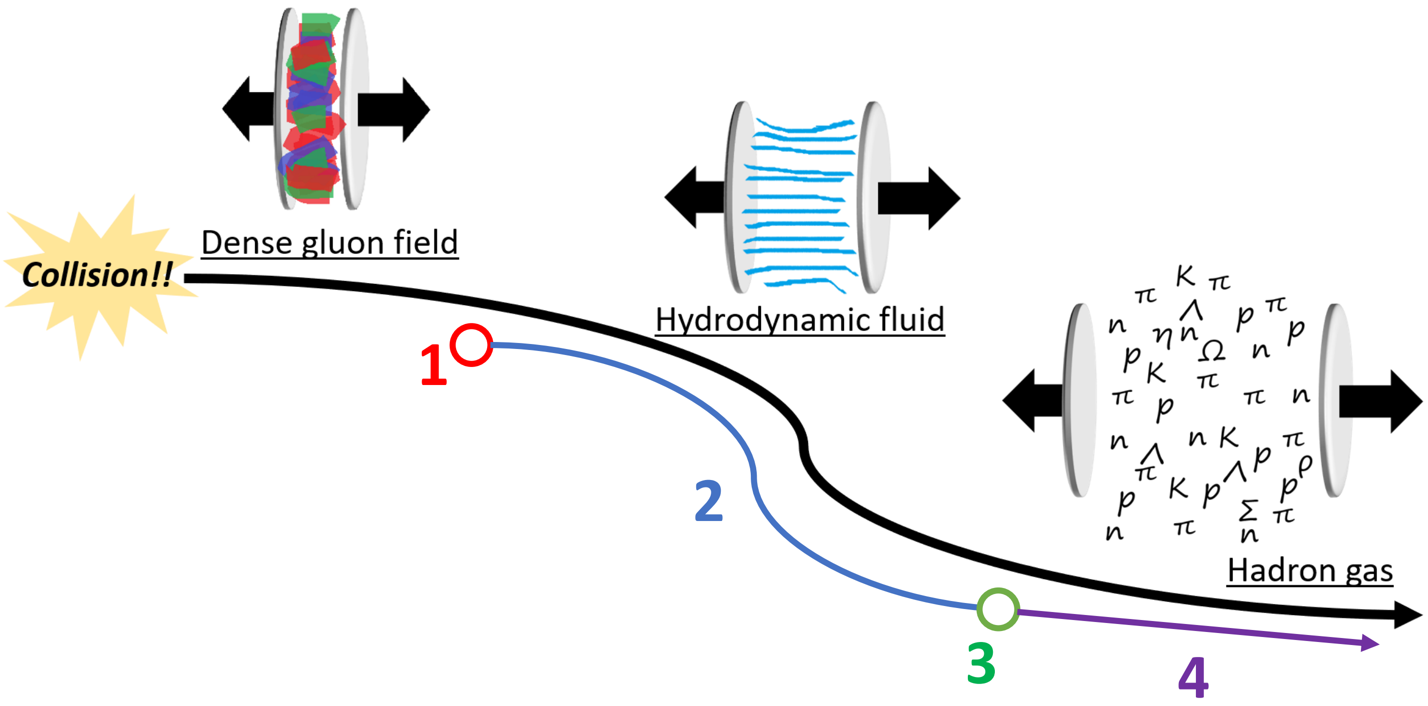

Phenomenological Analysis of the Evolution

1. Initial State Model

↓

2. Relativistic Hydrodynamic Simulation

↓

3. Cooper-Frye Formula

↓

4. Hadron Transport Model

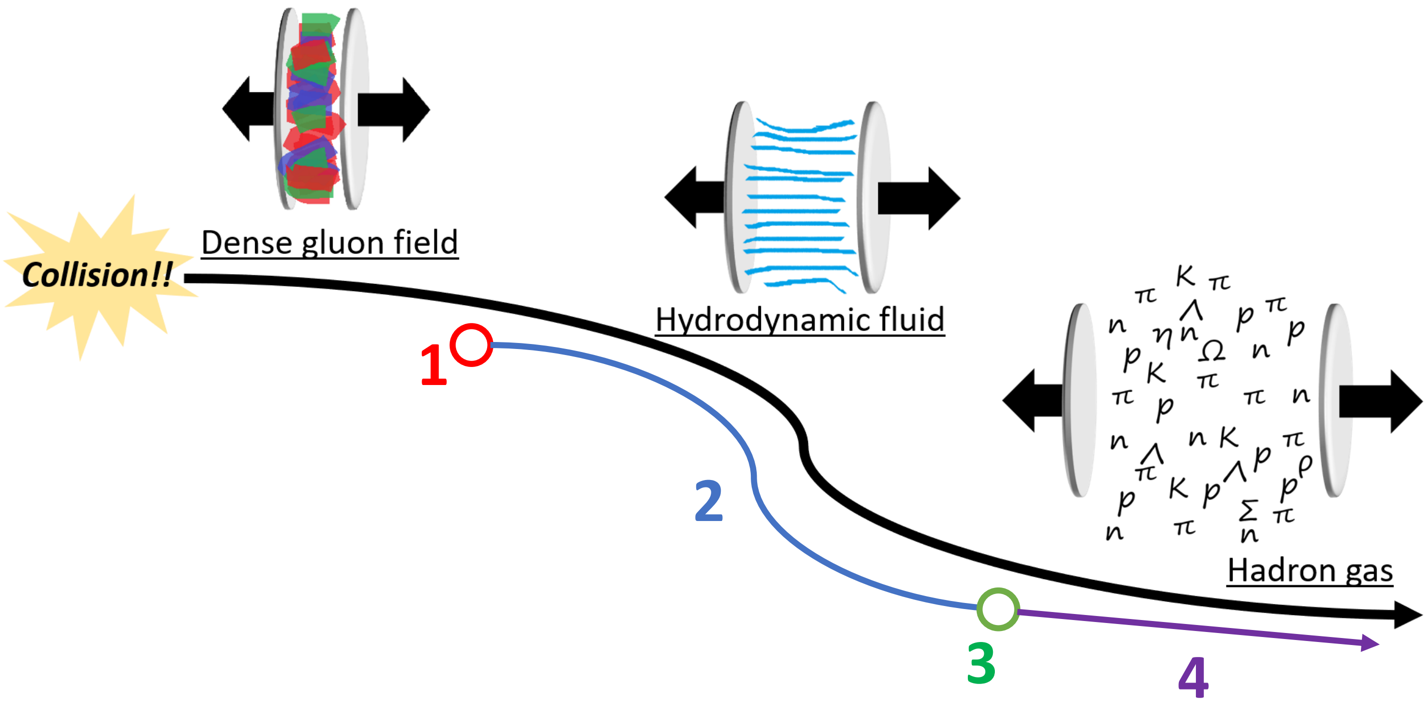

***Non-dynamical model*: providing hydrodynamic initial conditions directly**

- Monte Carlo Glauber model [M. L. Miller, *et al*. (2007)]
- Reduced Thickness Event-by-event Nuclear Topology (TRENTo)
  [J. S. Moreland, *et al*. (2015), W. Ke, *et al*. (2017)]
- …

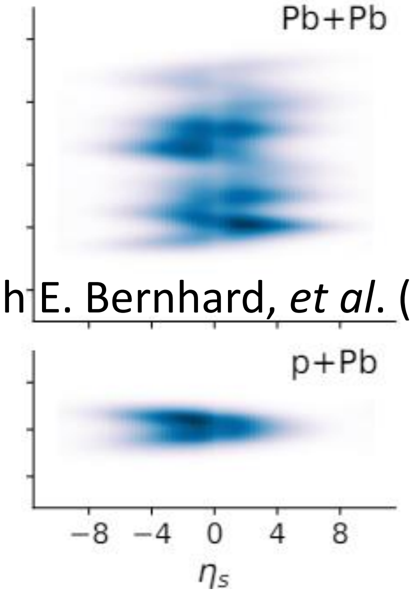

Jonah E. Bernhard, *et al*. (2016)

***Dynamical Model*: simulating pre-hydrodynamic stage + switching it into hydrodynamics fluid**

- IP-glasma model [B. Schenke, *et al*. (2012)]

  *** Degrees of freedom focused:**
  the dense "soft" gluon matter (glasma)

  *** Description of glasma:**
  classical Yang-Mills (CYM) equation of motion

- …

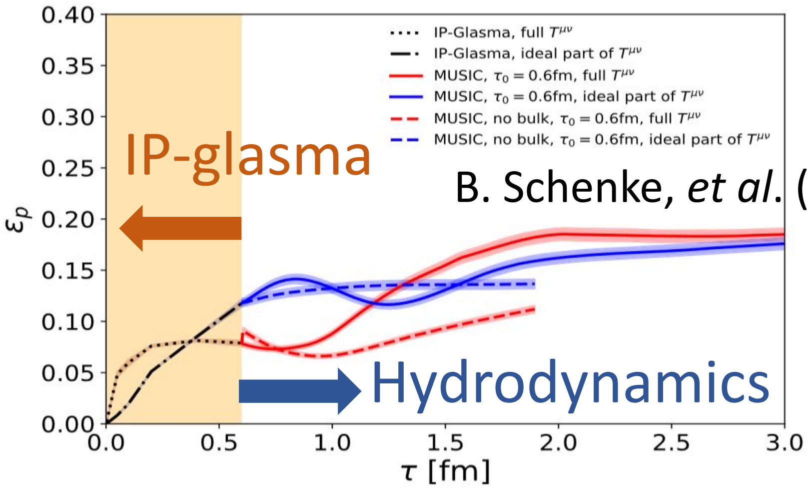

B. Schenke, *et al*. (2018)

Theoretical Background:

- Nucleus at high energy
  - * Gluon saturation: A number of gluons with small momentum fraction is very large and is characterized by Q_S
  - * HIC liberates a large amount of soft gluons (**glasma**)
- **Color Glass Condensate (CGC)**
  - * a theoretical state that captures features of a relativistic heavy-ion
  - * internal soft gluons = classical Yang-Mills (CYM) field $(\boldsymbol{A}, \boldsymbol{E})$
  - * internal hard colored particles = classical color charge density $(\boldsymbol{\rho})$ generated as event-by-event random number according to weight function $(\boldsymbol{W_Y[\rho]})$

    ↳ momentum rapidity for separation between "hard" and "soft"
  - * **Glasma is modeled using CYM field as well, which is generated by collision of two CGCs**

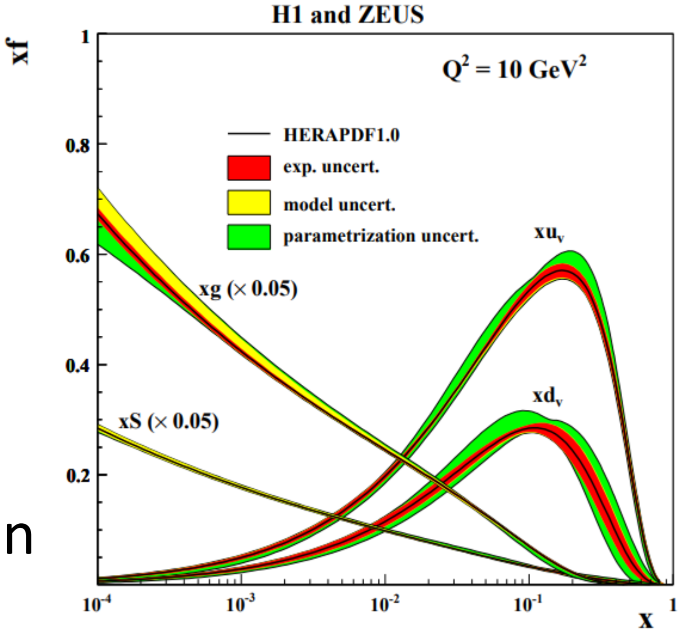

$$[D_\mu, F^{\mu\nu}] = \delta^{\nu+}\rho_A + \delta^{\nu-}\rho_B, \qquad [D_\mu, \delta^{\pm}\rho_{A/B}] = 0$$

*light cone coordinates, $x^{\mp} = (x \mp z)/\sqrt{2}$

IP-glasma model ②

- **Impact-Parameter-Saturation (IP-sat) model:**
Referring to phenomenological value of saturation scale $Q_s(x_{\mathrm{Bjoken}}, \vec{x}_\perp)$ to construct initial condition of CGC

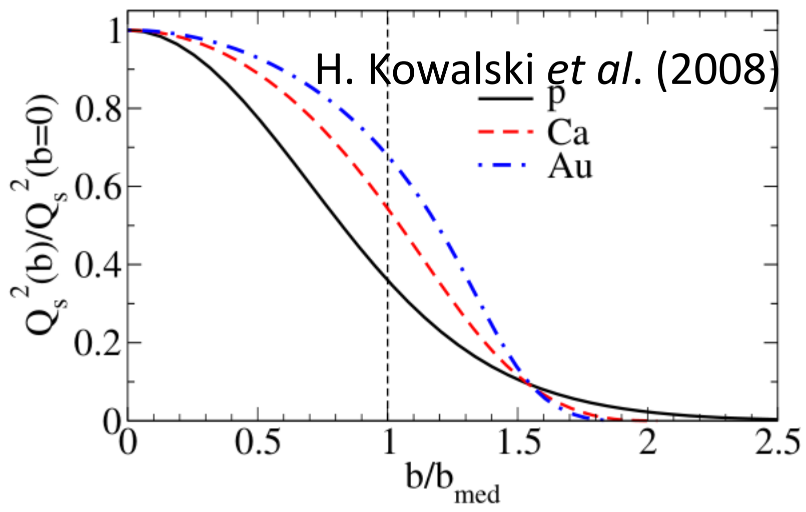

- **Boost invariant approximation:**
1. $W_Y[\rho]$, given as Gaussian function (McLerran-Venugopalan (MV) model)

2. Shockwave approximation:
(Infinitely thin) $\rho^A \propto \delta(x^-)$ and $\rho^B \propto \delta(x^+)$

(Frozen) $\partial_+\rho^A = 0$ and $\partial_-\rho^B = 0$

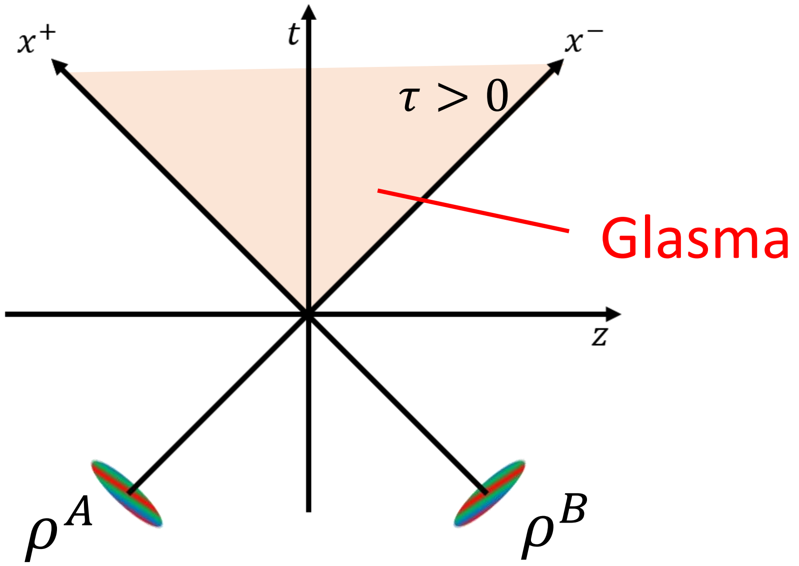

Study of Rapidity Dependence from Experiment and Theory

Experiment: rapidity dependent observables, and their decorrelation in rapidity direction

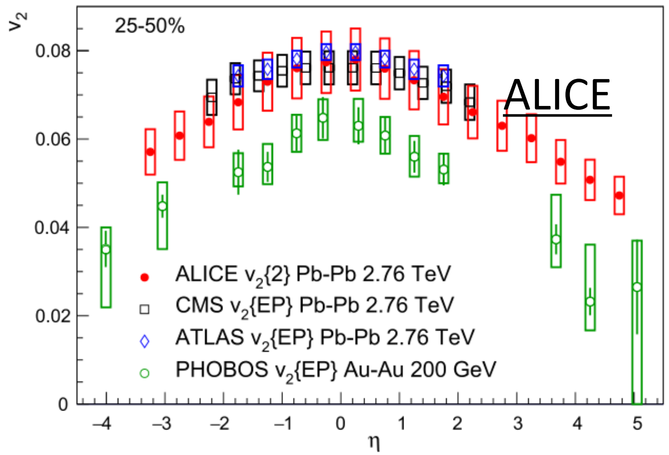

ALICE

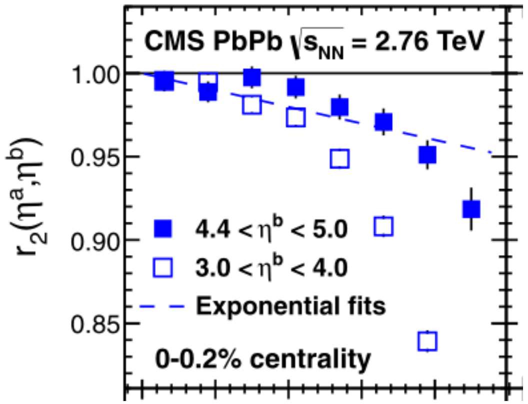

CMS

Theory:

development of phenomenological models where rapidity dependent effect is taken into acount

* AMPT(a multiphase transport model)

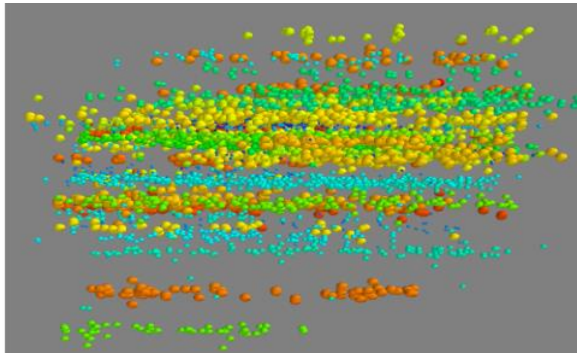

Long-Gang Pang, *et al.* (2016)

* TRENTo

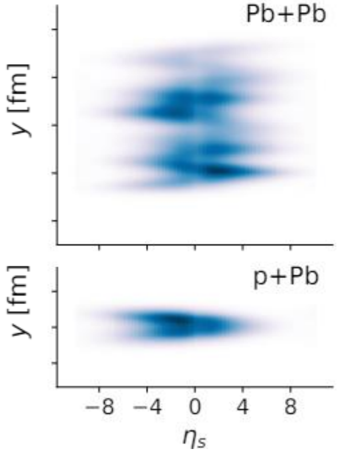

Jonah E. Bernhard, *et al.* (2016)

Direction of 3D Glasma

1. $\boldsymbol{W_Y[\rho]}$ ***for wide values of*** Y ***obtained by solving JIMWLK equation***

* B. Schenke, *et al.* (2016, 2022), S. McDonald, *et al.* (2019, 2023)

2. Relax shockwave approximation

- Finite thin ρ
  - T. Altinoluk, *et al.* (2014,2016, 2021,2022), G.A. Chirilli (2019,2021), P. Agostini, *et al.* (2019,2021,2022,2023), C. S. Lam, *et al.* (2000), S. Özönder, *et al.* (2014)

- Both finite thin and dynamical ρ
  - D. Gelfand, *et al*. (2016), A. Ipp, *et al*. (2017,2021,2024), S. Schlichting, *et al*. (2021), H. M. and X.-G. Huang (2023,2024)

Direction of 3D Glasma

1. $W_Y[\rho]$ for wide values of Y obtained by solving JIMWLK equation

* B. Schenke, *et al.* (2016, 2022), S. McDonald, *et al.* (2019, 2023)

2. Relax shockwave approximation

- Finite thin ρ
  - T. Altinoluk, *et al.* (2014,2016, 2021,2022), G.A. Chirilli (2019,2021), P. Agostini, *et al.* (2019,2021,2022,2023), C. S. Lam, *et al.* (2000), S. Özönder, *et al.* (2014)

- Both finite thin and dynamical ρ
  - D. Gelfand, *et al*. (2016), A. Ipp, *et al*. (2017,2021,2024), S. Schlichting, *et al*. (2021), H. M. and X.-G. Huang (2023,2024)

Analytic calculation: limited up to leading order

Direction of 3D Glasma

1. $W_Y[\rho]$ for wide values of Y obtained by solving JIMWLK equation

* B. Schenke, *et al.* (2016, 2022), S. McDonald, *et al.* (2019, 2023)

2. Relax shockwave approximation

- Finite thin ρ
  - T. Altinoluk, *et al.* (2014,2016, 2021,2022), G.A. Chirilli (2019,2021), P. Agostini, *et al.* (2019,2021,2022,2023), C. S. Lam, *et al.* (2000), S. Özönder, *et al.* (2014)

- Both finite thin and dynamical ρ
  - D. Gelfand, *et al.* (2016), A. Ipp, *et al.* (2017,2021,2024), S. Schlichting, *et al.* (2021), H. M. and X.-G. Huang (2023,2024)

Computational calculation: require much numerical resource

Direction of 3D Glasma

1. $W_Y[\rho]$ for wide values of Y obtained by solving JIMWLK equation

* B. Schenke, *et al.* (2016, 2022), S. McDonald, *et al.* (2019, 2023)

2. Relax shockwave approximation

- Finite thin ρ
  - T. Altinoluk, *et al.* (2014,2016, 2021,2022), G.A. Chirilli (2019,2021), P. Agostini, *et al.* (2019,2021,2022,2023), C. S. Lam, *et al.* (2000), S. Özönder, *et al.* (2014)

- Both finite thin and dynamical ρ
  - D. Gelfand, *et al.* (2016), A. Ipp, *et al.* (2017,2021,2024), S. Schlichting, *et al.* (2021), H. M. and X.-G. Huang (2023,2024)

3D glasma simulation beyond shockwave approximation have not yet reached stage of phenomenological applications!!

Computational calculation: require much numerical resource

Direction of 3D Glasma

1. $W_Y[\rho]$ for wide values of Y obtained by solving JIMWLK equation

* B. Schenke, *et al.* (2016, 2022), S. McDonald, *et al.* (2019, 2023)

2. Relax shockwave approximation

- Finite thin ρ
  - T. Altinoluk, *et al.* (2014,2016, 2021,2022), G.A. Chirilli (2019,2021), P. Agostini, *et al.* (2019,2021,2022,2023), C. S. Lam, *et al.* (2000), S. Özönder, *et al.* (2014)

- Both finite thin and dynamical ρ
  - D. Gelfand, *et al*. (2016), A. Ipp, *et al*. (2017,2021,2024), S. Schlichting, *et al*. (2021), H. M. and X.-G. Huang (2023,2024)

✔ **We have recently developed efficient 3D glasma simulation method**

✔ **Today, we apply our method to early stage of Au-Au collisions at RHIC**

Table of Contents

“Usual” and “Modified” Milne Coordinates

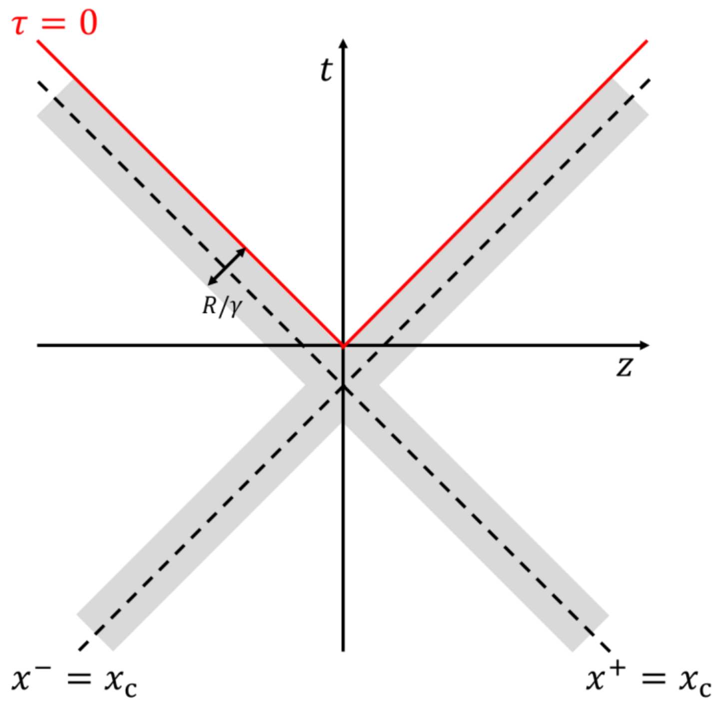

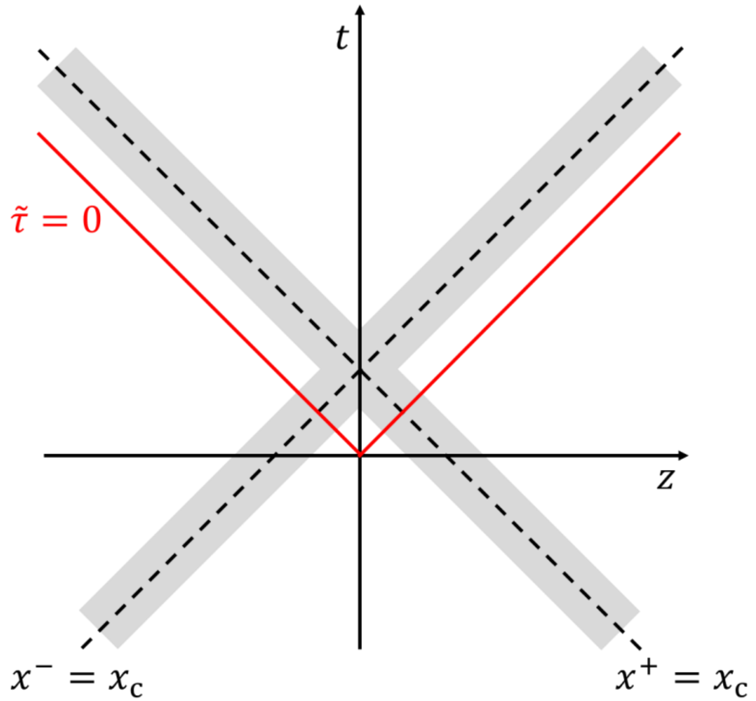

1. Usual Milne coordinates for observation:

$$\tau = \sqrt{2\left(x^- - x_c - \frac{R}{\sqrt{2}\gamma}\right)\left(x^+ - x_c - \frac{R}{\sqrt{2}\gamma}\right)}$$

$$\eta = \frac{1}{2}\ln\frac{x^+ - x_c - R/[\sqrt{2}\gamma]}{x^- - x_c - R/[\sqrt{2}\gamma]}$$

2. Modified Milne coordinates for simulation:

$$\tilde{\tau} = \sqrt{2x^- x^+}, \quad \tilde{\eta} = \frac{1}{2}\ln\frac{x^+}{x^-}$$

4 steps in numerical calculation

1. Put initial condition of two incoming nuclei on lattice before the collision

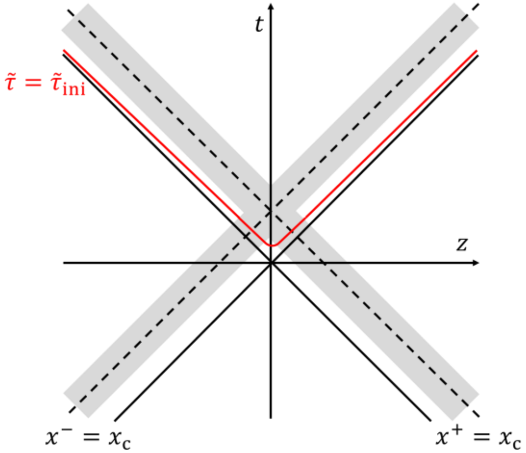

$$\left.(A, E, \rho^i)\right|_{\tilde{\tau}=\tilde{\tau}_{\rm ini}}$$

2. Evolve the CYM field and classical color charges numerically

$$\left[D_\mu, F^{\mu\, i=1,2,\tilde{\eta}}\right] = J^{i=1,2,\tilde{\eta}}, [D_\mu, J^\mu] = 0$$

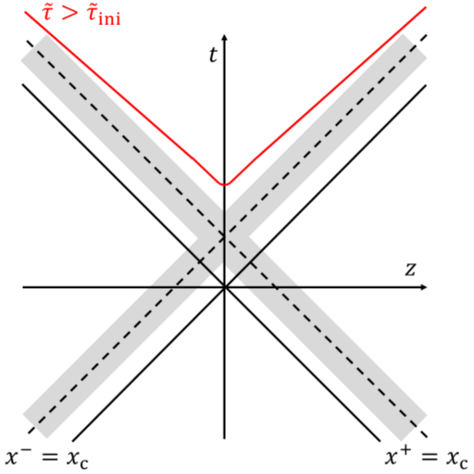

3. Get observables for Usual Milne coordinates

$$T^{\tilde{\mu}\tilde{\nu}}(\tilde{\tau}, \tilde{\eta}) \quad \rightarrow \quad T^{\mu\nu}(\tau, \eta)$$

4. Repeat 1~3 and take event-average

$\langle T^{\mu\nu} \rangle_{\rm eve}$ (~ensemble average over W_Y)

Initial Condition of CYM field

- Incoherent sum of solutions for each single nuclei + small modification for $E^{\tilde{\eta}}$

$$A_i = A_i^A + A_i^B, \quad E^{\mathrm{i}} = E^{Ai} + E^{Bi}$$
$$A_{\tilde{\eta}} = 0, \quad E^{\tilde{\eta}} = i[A_i^A, A_i^B]$$

*Fock-Schwinger gauge: $A^{\tilde{\tau}} = 0$

$A_i^{A/B}, E^{A/B\,i}$: Solution of E.O.M. for single nucleus

$E^{\tilde{\eta}} = i[A_i^A, A_i^B]$:
made to satisfy Gauss law ($\left[D_\mu, F^{\mu\tilde{\tau}}\right] = x^- \rho^A + x^+ \rho^B$)

3D Nucleus Model: Formulation

2D IP-glasma initial condition

- MV model: $< \rho_i^{A/B,a}(\overrightarrow{x_\perp})\rho_j^{A/B,b}(\overrightarrow{x_\perp}') > = \delta^{ij}\delta^{ab}\left(g^2\mu\left(\frac{\overrightarrow{x_\perp}+\overrightarrow{x'_\perp}}{2}\right)\right)^2 \delta^2(\overrightarrow{x_\perp}-\overrightarrow{x'_\perp})$
- Nucleus saturation scale based on IP-sat model: $\left(g^2\mu(\overrightarrow{x_\perp})\right)^2 \propto \left(Q_{s,A}(\overrightarrow{x_\perp})\right)^2$

3D IP-glasma initial condition

- Nucleus color charge density = incoherent sum of nucleon's one: $\rho_{\mathrm{tot}}^{A/B} = \sum_{i=1}^{N_{\mathrm{A}}=197} \rho_i^{A/B}$
- MV model: $< \rho_i^{A/B,a}(x^{\mp},\overrightarrow{x_\perp})\rho_j^{A/B,b}(x'^{\mp},\overrightarrow{x_\perp}') >$

$$= \delta^{ij}\delta^{ab}\left(g^2\mu_{3\mathrm{D}}\left(\frac{x^{\mp}+x'^{\mp}}{2}-b_i^{\mp},\frac{\overrightarrow{x_\perp}+\overrightarrow{x'_\perp}}{2}-\overrightarrow{b_{\perp,i}}\right)\right)^2 N_{1\mathrm{D}}(x^- - x'^-; l_{\mathrm{L}})\delta^2(\overrightarrow{x_\perp}-\overrightarrow{x'_\perp})$$

Longitudinal correlation length

* Gaussian shape in longitudinal direction: $g^2\mu(x^{\mp},\overrightarrow{x_\perp}) \propto N_{1D}({x^{\mp}}^2, r_L)$

*$\left(g^2\mu(\vec{x})\right)^2 = \int dx^{\mp}\left(g^2\mu_{3\mathrm{D}}(\vec{x})\right)^2 \propto \left(Q_{s,n}(\overrightarrow{x_\perp})\right)^2$

3D Nucleus Model: Model Parameters

Determination of four parameters for mimicking Au-Au collision at RHIC

1. Bjorken x for determination of $Q_{s,n}$

$$\left[\begin{array}{l} x_{\mathrm{Bjorken}} \sim \frac{p_\perp}{\sqrt{s_{NN}}} \text{ [relation for } \mathrm{Y} \sim 0] \\ < p_\perp >\sim 1 \text{ GeV} \\ \sqrt{s_{NN}} = 200 \text{ (GeV)} \end{array}\right. \Longrightarrow \quad x_{\mathrm{Bjorken}} \sim 0.01$$

2. Longitudinal extent of ρ, r_L

ρ consists of hard partons with larger x_{Bjorken} $\Longrightarrow$ $r_L \sim \left[2x_{\mathrm{Bjorken}}\sqrt{s_{NN}}\right]^{-1}$

3. Ratio, $\lambda = g^2\mu/Q_{s,n}$
4. Longitudinal correlation length, l_L

$\Longrightarrow$ **tuned by referring to observables**

Table of Contents

Table of Contents

Table of Contents

Q_s

ε, N_{CS}, n_5

$\varepsilon, \varepsilon_n, T^{\tau 3}, L, \omega$

Q_s of Single Nucleus

Saturation scale of nucleus $Q_{s,A}$

- Wilson line correlator for transverse translational invariant glasma [T. Lappi (2008)]

$$C(k_t) = \int d^2x_t \langle \left| \mathrm{Tr}\left[U^\dagger(\boldsymbol{x}_t + \boldsymbol{y}_t) U(\boldsymbol{y}_t) \right] \right|^2 - 1 \rangle e^{i\boldsymbol{k}_t \cdot \boldsymbol{x}_t} \qquad \left(U(\mathbf{x}_T) = P e^{\mathrm{i}\int \mathrm{d}x^- A^+} \right)$$

- Q_s can be defined as value of transverse momentum where peak structure appears

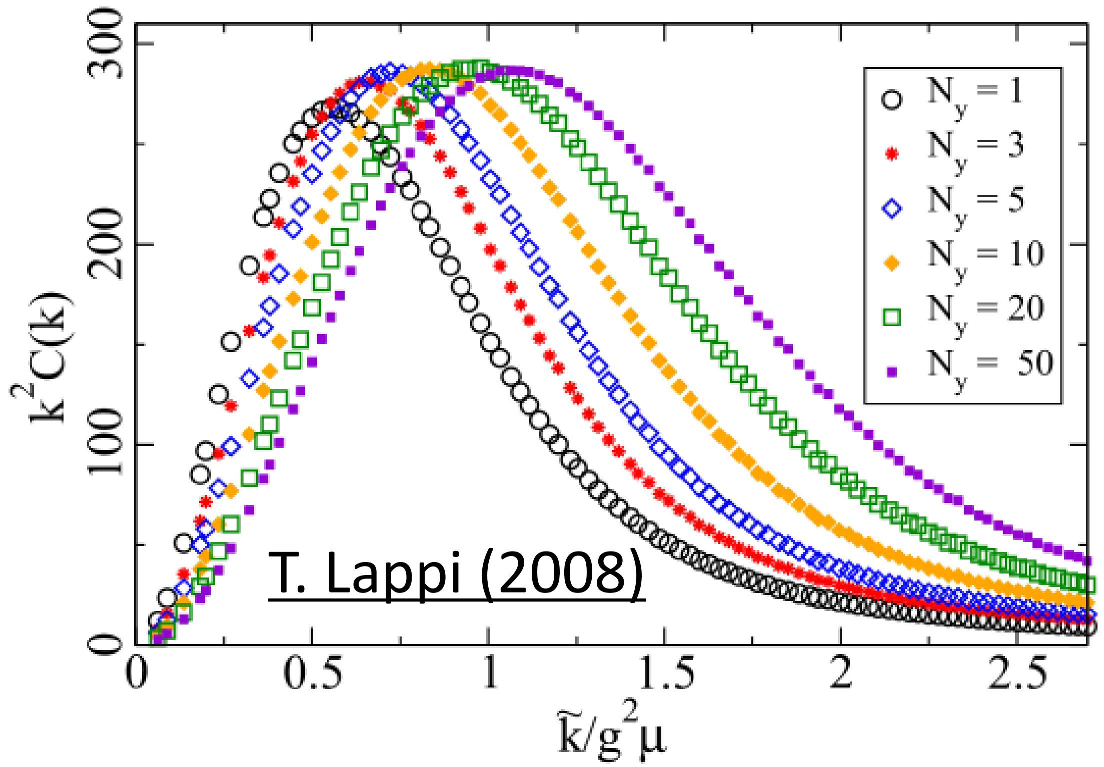

Q_s of Single Nucleus

- Utilizing approximate transverse translational invariance, we can estimate $Q_{s,A}$ for center region of nucleus

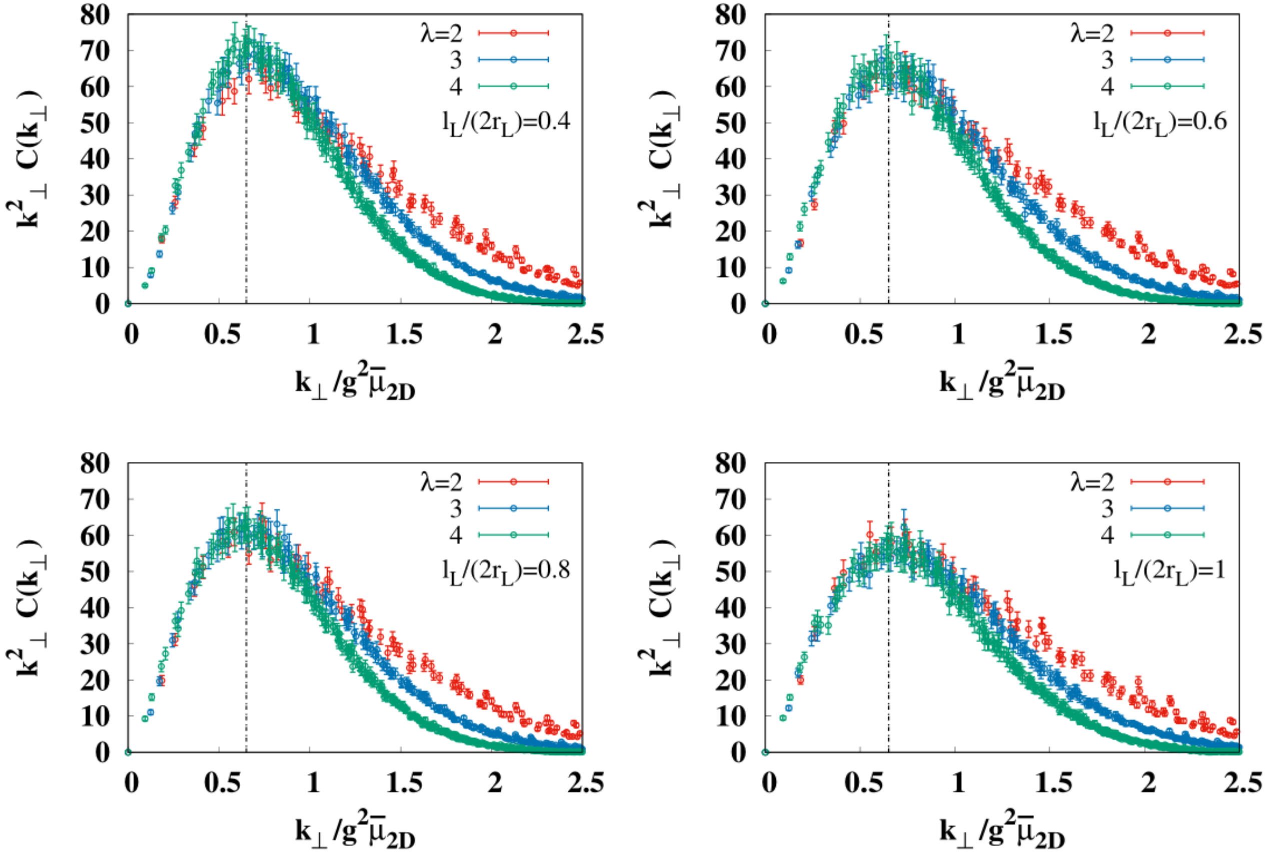

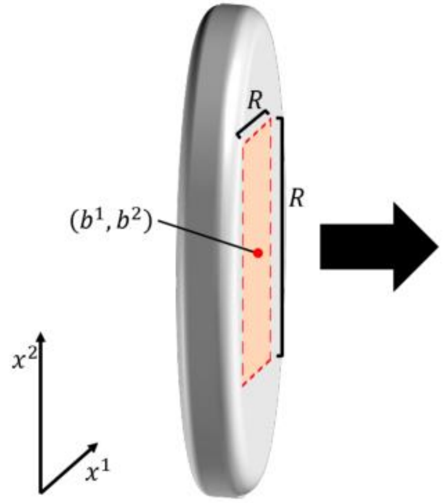

✔ $Q_{s,A}^{\text{est.}} = 0.65\, g^2\mu_{2\text{D}} = 0.346\lambda$ GeV for $l_\text{L}/2r_\text{L}$=0.4-1.0 and $\lambda = 2-4$

✔ $\lambda = 3.18$ reproduces phenomenological value of $Q_{s,A} = 1.1$ GeV

[N. Armesto (2002)]

* $g^2\mu_{2D} \sim 0.532\lambda$ GeV: maximum value of $g^2\mu(\overrightarrow{x_\perp})$

Energy density in local rest frame: $T^{\mu}_{\nu}u^{\nu} = \varepsilon_{\mathrm{LRF}}u^{\mu}$

- We assume $u_{\perp} = 0$ and extract $\varepsilon_{\mathrm{LRF}}$ from $\varepsilon_{\mathrm{LRF}} = \frac{1}{2}\left([T^{\tau\tau} - T^{\eta\eta}] + \sqrt{[T^{\tau\tau} + T^{\eta\eta}]^2 - 4[T^{\tau\eta}]^2}\right)$
- Note: CYM field of single nucleus (Weizsäcker-Williams field) strictly yields zero $\varepsilon_{\mathrm{LRF}}$

✔ As l_{L} decreases, shape of $\varepsilon_{\mathrm{LRF}}$ changes from a rounded one to dip structure

✔ Later, we use $l_{\mathrm{L}} = 0.6$ and 1.0

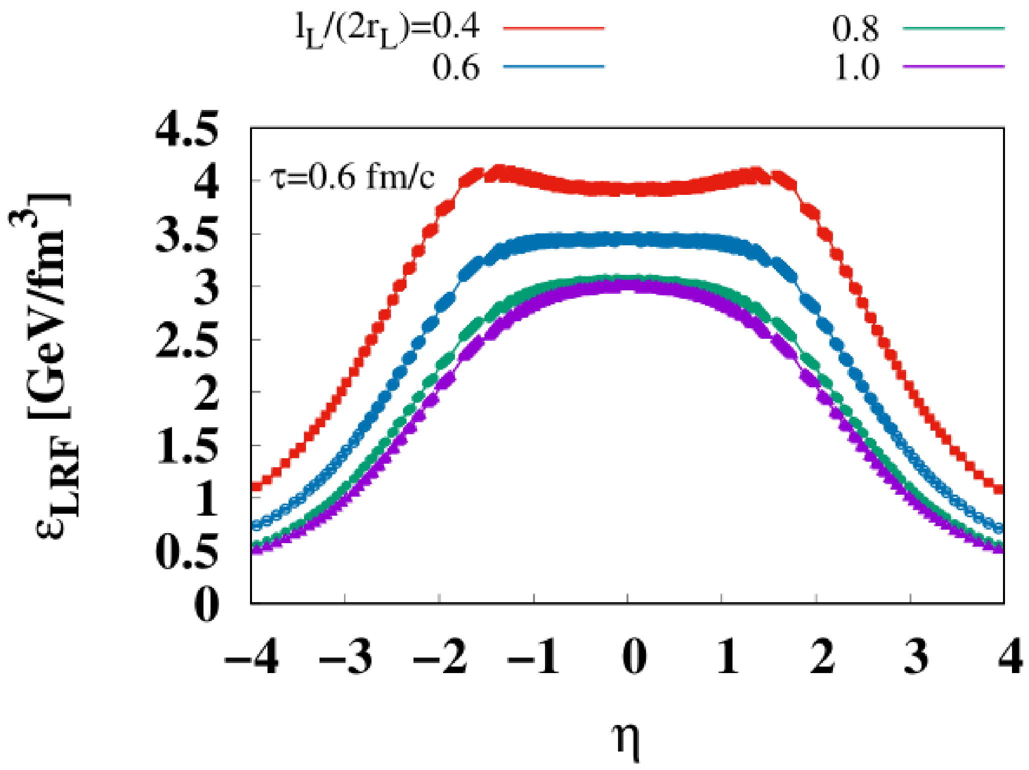

Transverse Profile of $\varepsilon_{\mathrm{LRF}}$ at Central Collisions

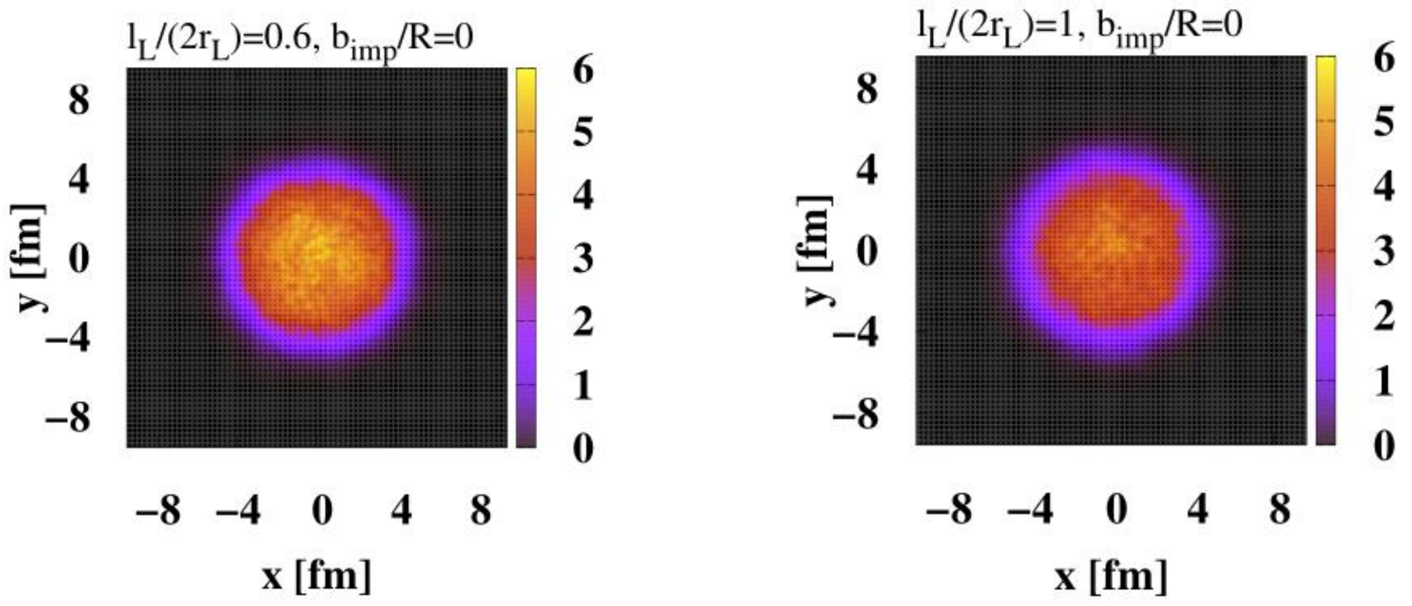

Mid-rapidity!!

- * $\varepsilon_{\mathrm{LRF}}$ in the center of figures: $\varepsilon_{\mathrm{LRF}} \sim 6\ \mathrm{GeV/\ fm^3}$

  * Boost-invariant hydrodynamic simulations [U. W. Heinz *et al*. (2002)]:
  $\varepsilon_{\mathrm{LRF}} \sim 11\ \mathrm{GeV/\ fm^3}$

  * Boost-invariant glasma simulation with MV model [A. Krasnitz *et al*. (2003)]:
  $7.1\ \mathrm{GeV/\ fm^3} \leq \varepsilon_{\mathrm{LRF}} \leq 40\ \mathrm{GeV/\ fm^3}$

- This discrepancy should be improved when $\mathrm{N_c} = 2 \rightarrow 3$.

Rapidity Profile of Squared N_{cs} at Central Collisions

Topological charge density

$$n_{\mathrm{T}} \equiv \frac{1}{8\pi^2}\mathrm{Tr}\boldsymbol{E}\cdot\boldsymbol{B}$$

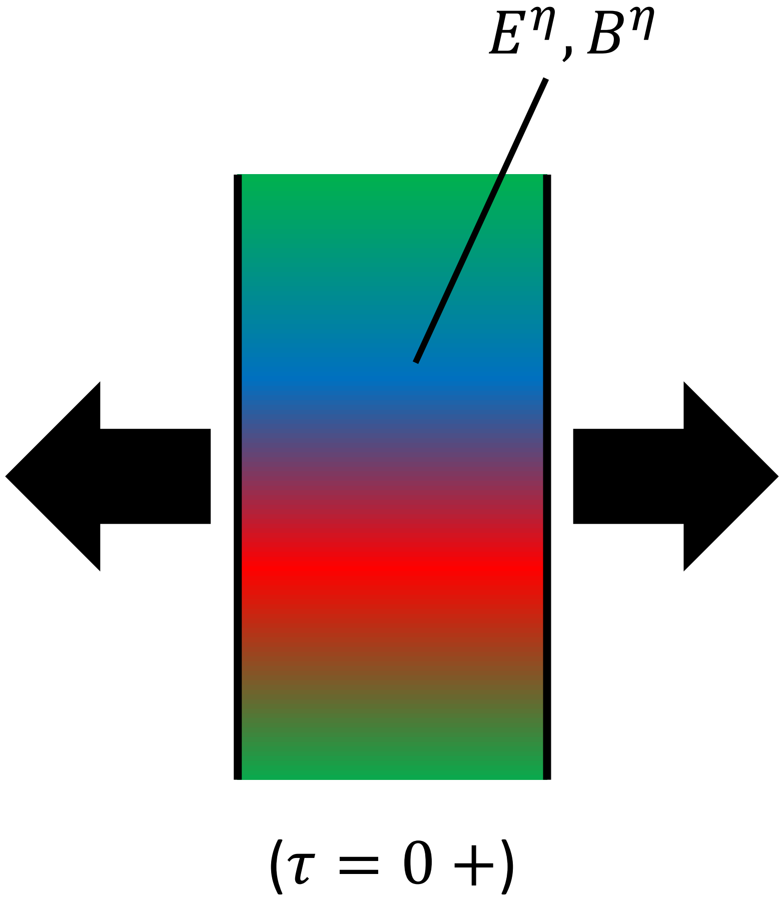

- 2D glasma initial condition shows strong parallel longitudinal colorelectric and colormagnetic fields emerge between WW fields just after collisions

➡ Generation of $\langle n_{\mathrm{T}}^2\rangle$ *!!*

- What happens for 3D glasma?

Rapidity Profile of Squared N_{cs} at Central Collisions

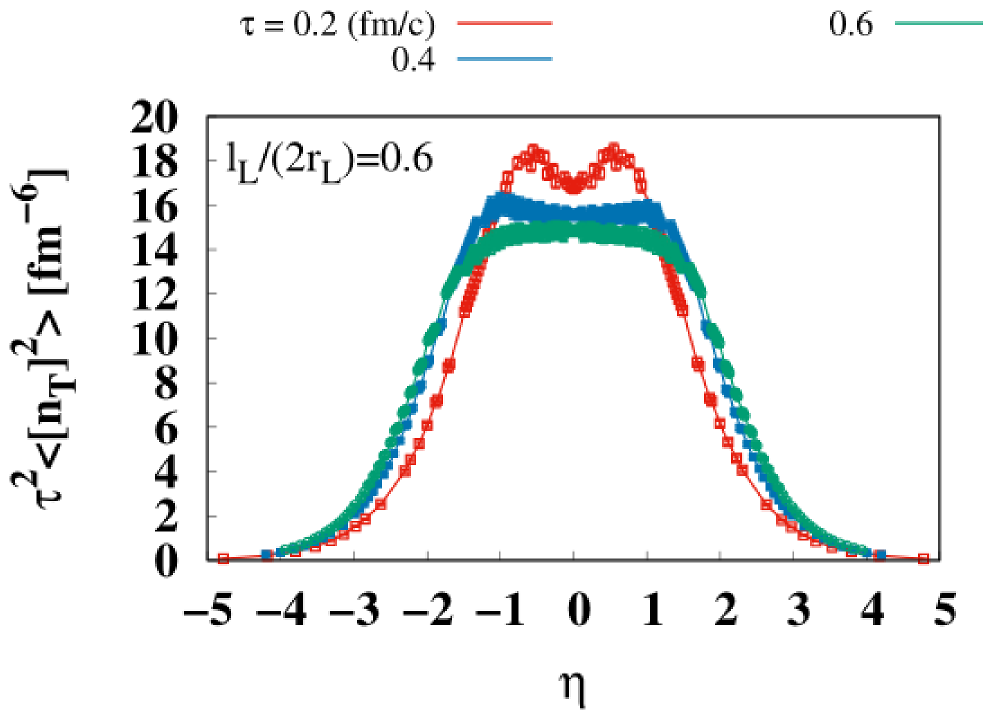

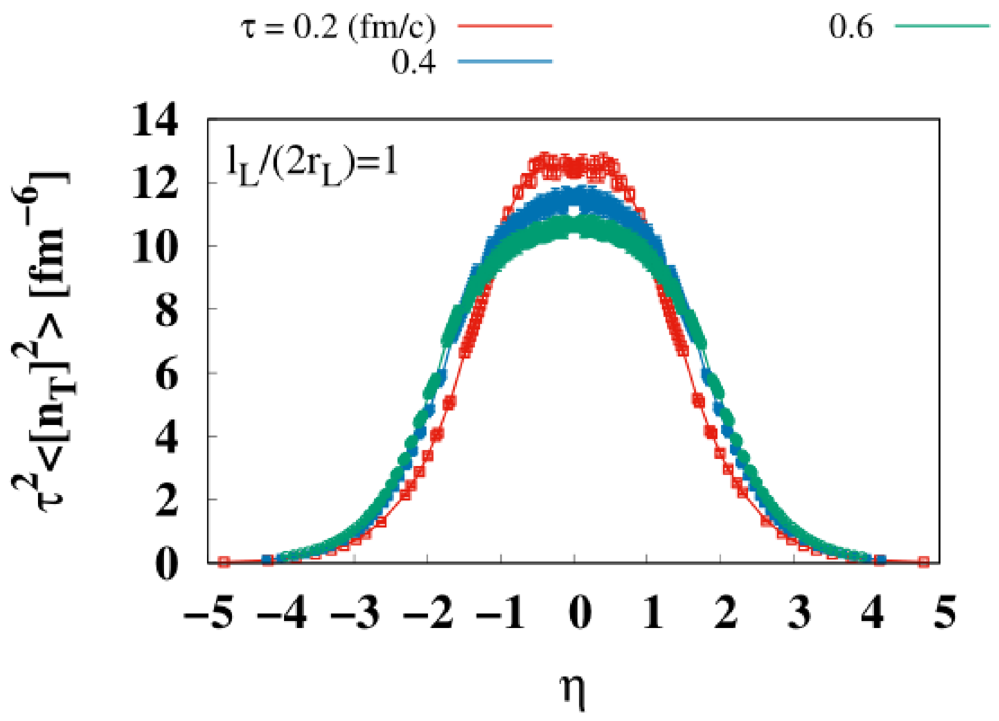

✔ Topological charge fluctuations are generated around mid-rapidity by the collision, with a shape similar to the LRF energy density

Transverse Correlation of n_5 at Central Collisions

Axial charge density

$$n_5 \equiv \tau j_5^\tau$$

- Adler-Bell-Jackiw anomaly equation tells us that the topological charge density is related to the divergence of the axial current

$$\partial_\tau(\tau j_5^\tau) - \tau \sum_{i=1,2,\eta} \partial_i j_5^i = \tau n_\mathrm{T}$$

- To estimate n_5, we focus on the central area the transverse plane and at mid-rapidity ($\eta = 0$), and assume $\left\langle j_5^{i=1,2,\eta} \right\rangle = 0$

$$n_5 = \int^\tau d\tau\ \tau n_\mathrm{T}$$

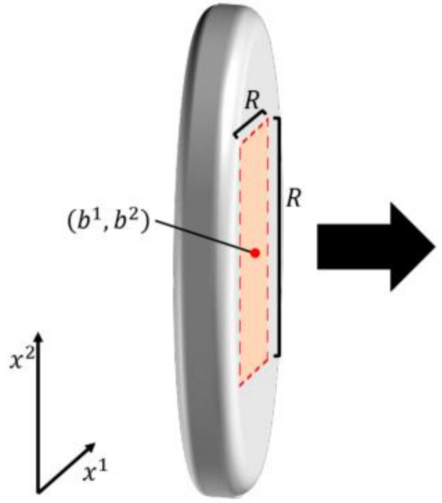

Transverse Correlation of n_5 at Central Collisions

- $D_\perp(r_\perp = |\boldsymbol{x}_\perp - \boldsymbol{y}_\perp|) \equiv \langle n_5(x^1, x^2) n_5(y^1, y^2) \rangle$

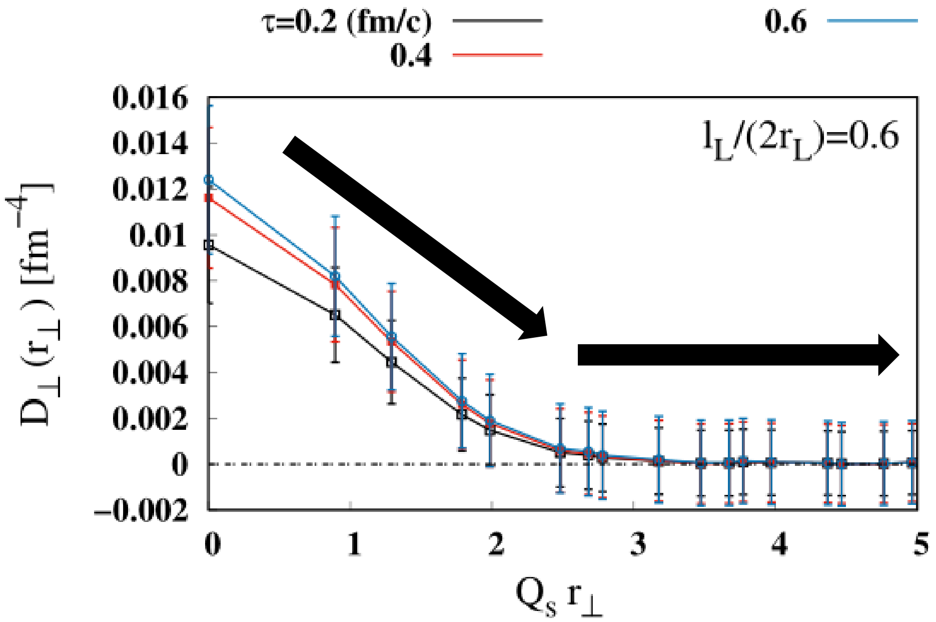

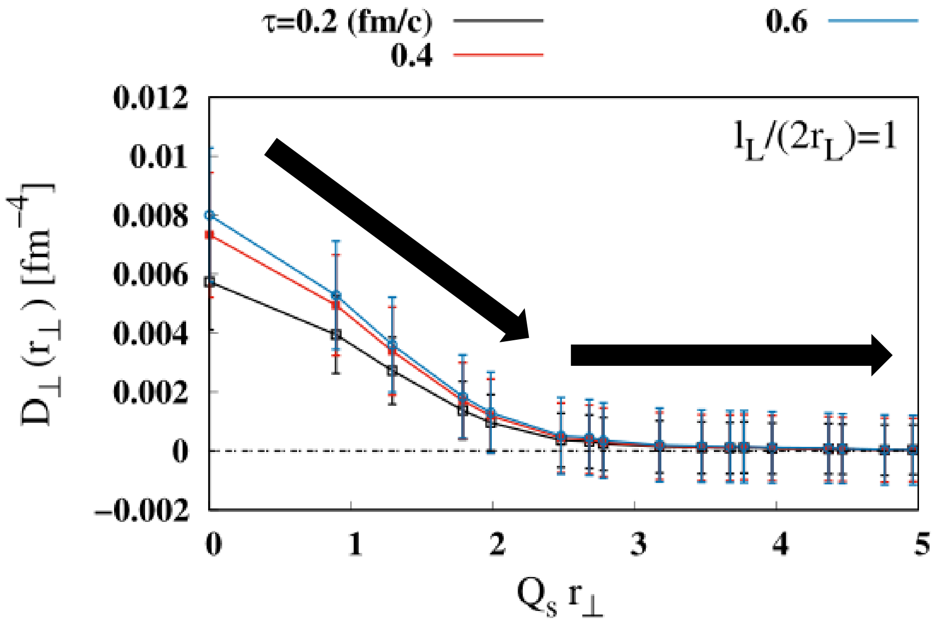

- ✔ $D_\perp$ decreases in $Q_s r_\perp < 3$, and is consistent with zero within the error in $Q_s r_\perp < 3$
- ✔ This behavior of $D_\perp$ does not change over proper time evolution
- ✔ This behavior and even magnitude of $D_\perp$ are in qualitative agreement with previous studies on the boost-invariant glasma [M. R. Jia *et al*. (2021)]

Transverse Profile of $\varepsilon_{\mathrm{LRF}}$ at Non-Central Collisions

- $\varepsilon_{\mathrm{LRF}}$ at central collision ($b_{\mathrm{imp}}/R = 0$) are isotropic in transverse plane
- $\varepsilon_{\mathrm{LRF}}$ at non-central collision with $b_{\mathrm{imp}}/R = 1$ have an anisotropic shape that looks elliptical
- The $\varepsilon_{\mathrm{LRF}}$ deformation is expected to reflect shape of overlap region of colliding nuclei

Mid-rapidity!!

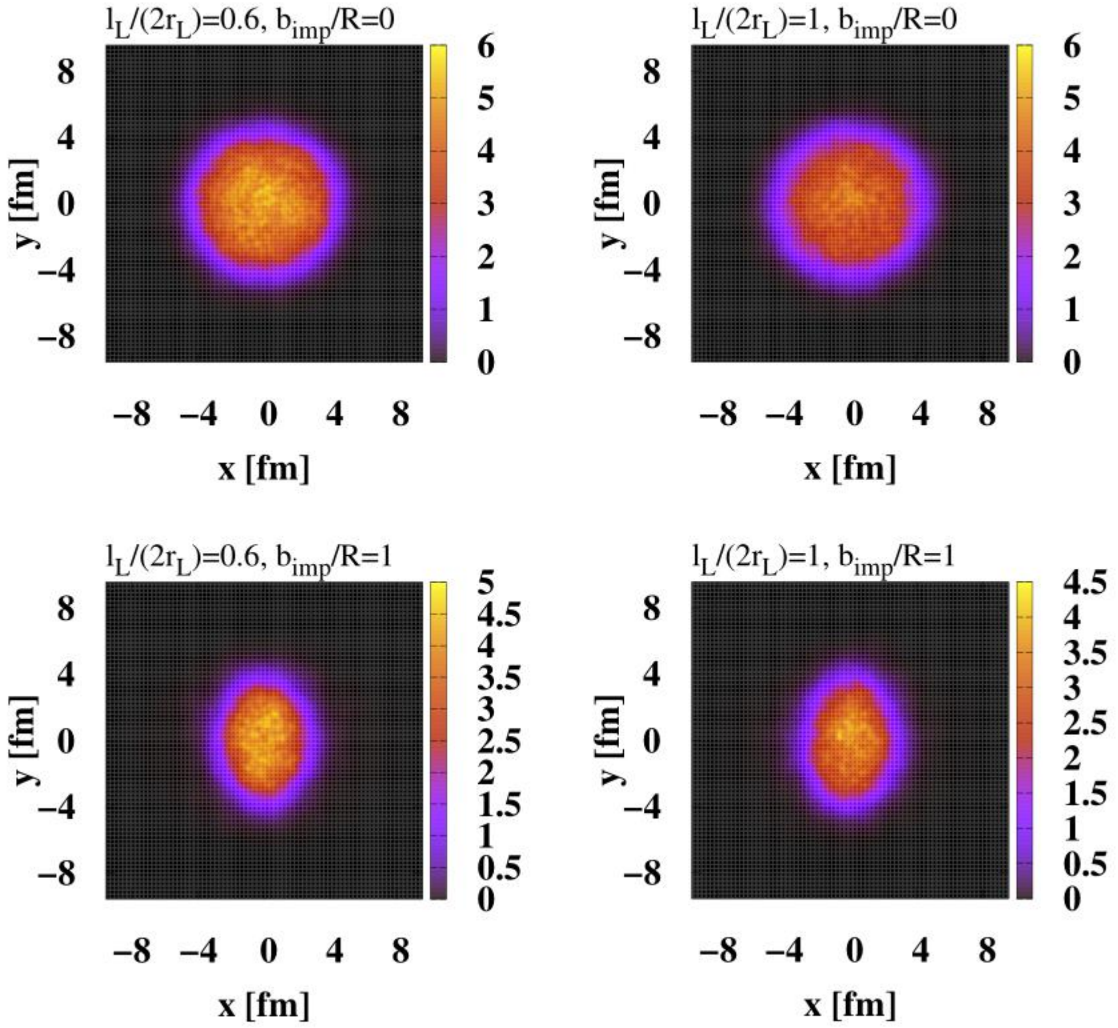

Eccentricity ε_n at Non-Central Collisions

Eccentricity

$$\varepsilon_n = \frac{\int d^2\boldsymbol{x}_\perp \varepsilon_{\mathrm{LRF}} r_\perp^n e^{in\phi}}{\int d^2\boldsymbol{x}_\perp \varepsilon_{\mathrm{LRF}} r_\perp^n}$$

$$\left[\begin{array}{l} \phi \equiv \arctan\left(x^2/x^1\right) \\ r_\perp \equiv \sqrt{(x^1)^2 + (x^2)^2} \end{array}\right.$$

- ε_n characterizes spatial anisotropy of a produced matter in the transverse plane perpendicular to the collision axis
- ε_2 characterizes elliptical deformation
- ε_n is expected to be converted into anisotropic flow (such as the elliptic flow which is a response to ε_2 during the system's collective evolution in the hydrodynamic stage

Rapidity Profile of ε_n at Non-Central Collisions

<u>Eccentricity</u>

- In central collisions, $\mathrm{Re}[\varepsilon_2]$ and $\mathrm{Re}[\varepsilon_4]$ are consistent with zero within the error
- As b_{imp} increases $\mathrm{Re}[\varepsilon_2]$ and $\mathrm{Re}[\varepsilon_4]$ become non-zero, indicating the formation of an anisotropic shape of the glasma
- consistent with the shape of $\varepsilon_{\mathrm{LRF}}$

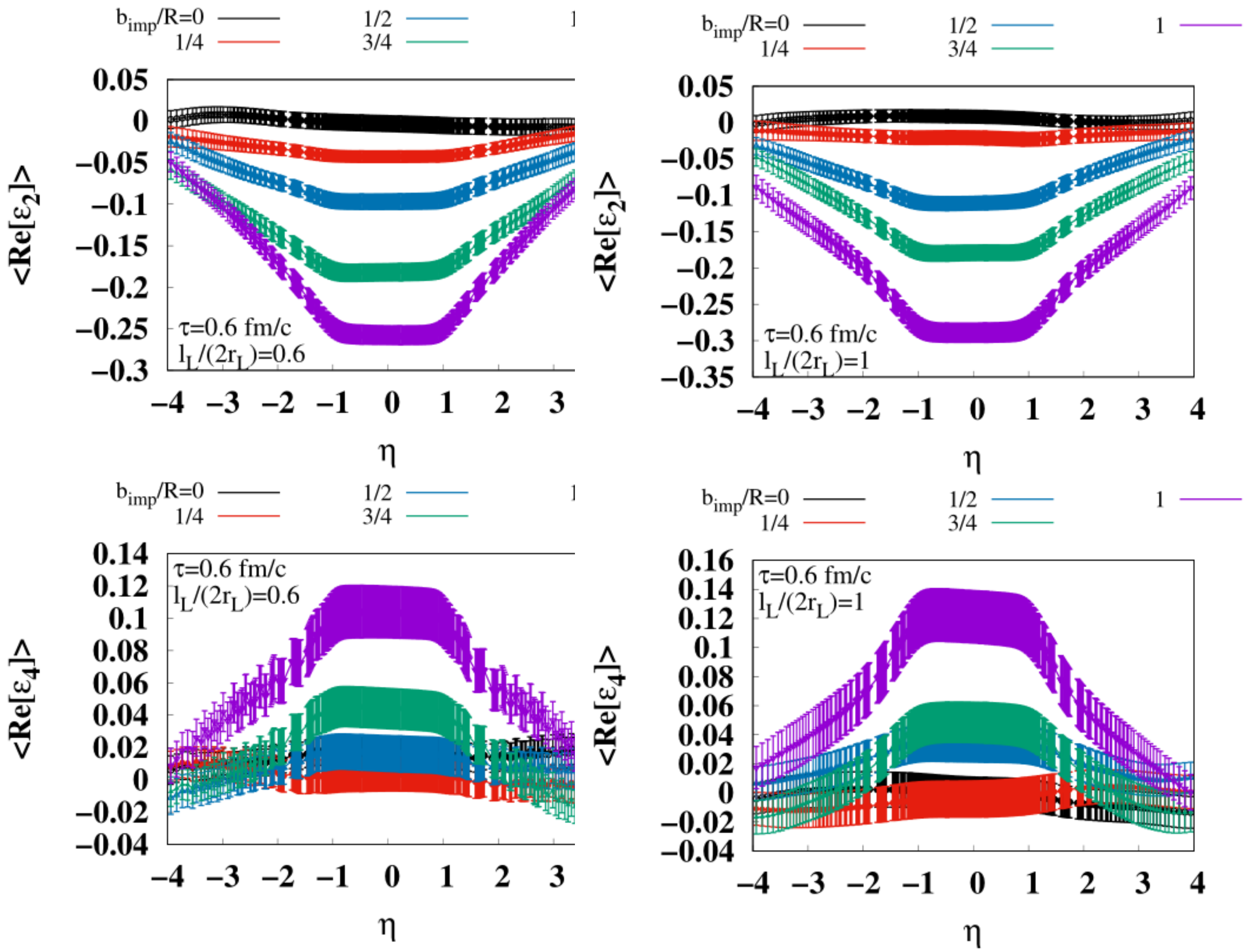

Rapidity Correlation of ε_n at Non-Central Collisions

- $\langle \mathrm{Re}\varepsilon_n(\eta)\mathrm{Re}\varepsilon_n(4)\rangle$

✔ For $b_{\mathrm{imp}} = 0$, the rapidity correlation is found to be a monotonic increasing function of η, which is expected to reflect the decorrelation effect that increases with the distance between two observed rapidities

✔ As b_{imp} increases, an enhancement around $\eta = 0$ gradually emerges, reflecting the increase in the magnitude of the eccentricity

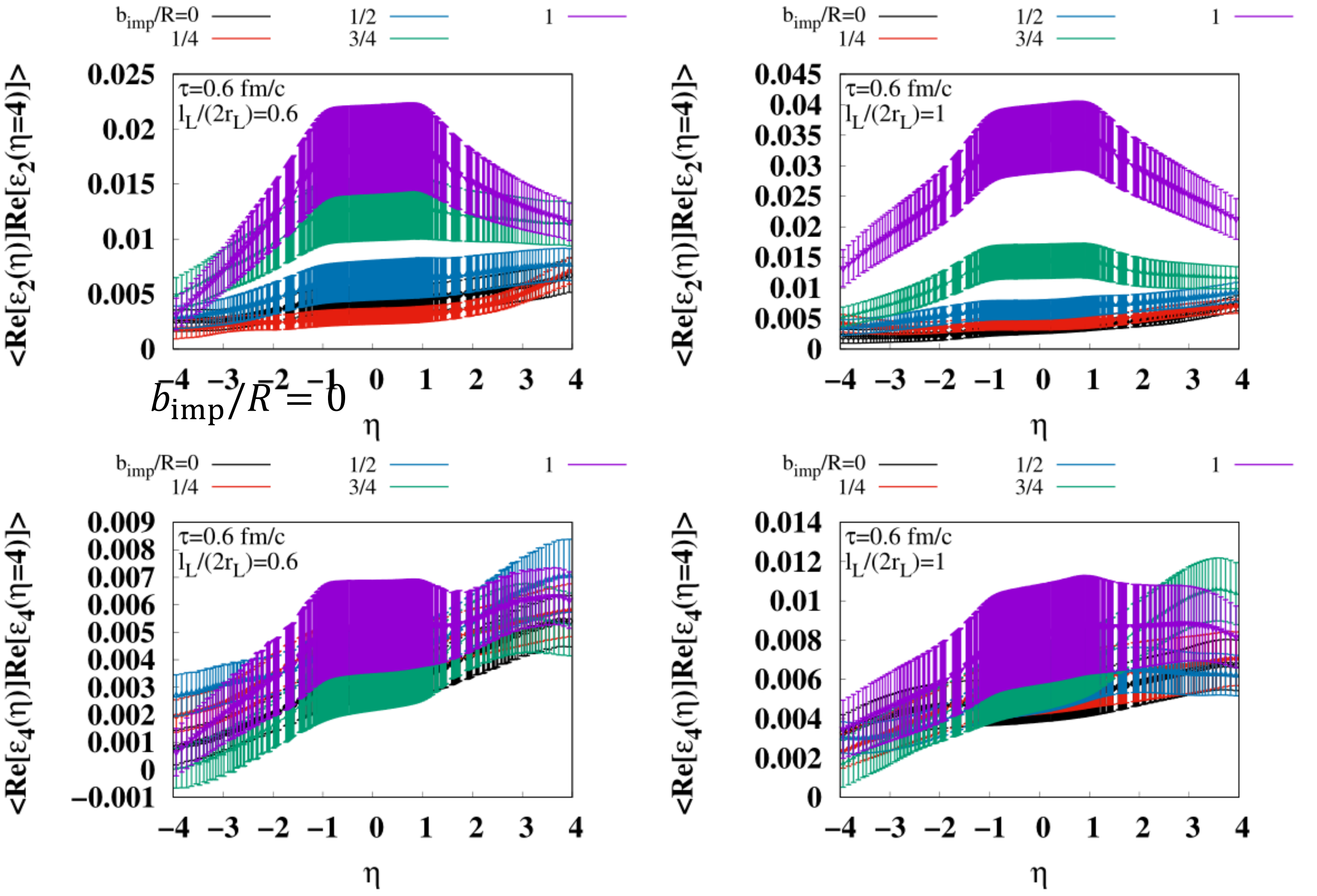

Reaction Plane Profile of $\varepsilon_{\mathrm{LRF}}$ at Non-Central Collisions

- Glasma generated in non-central collisions seems to expand diagonally

→ Pointing vector along collision axis create angular moment perpendicular to reaction plane?

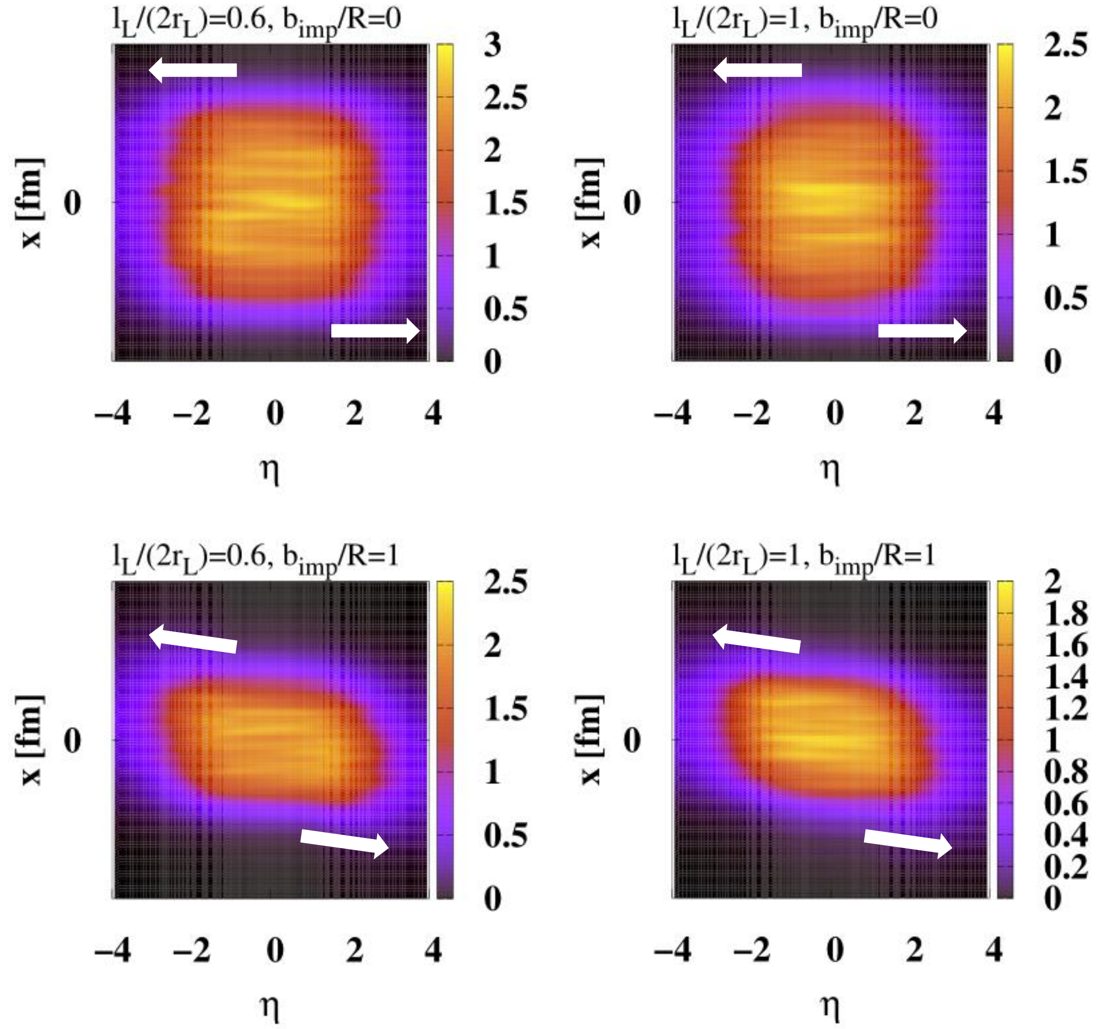

Rapidity Profile of $T^{\tau 3}$ at Non-Central Collisions

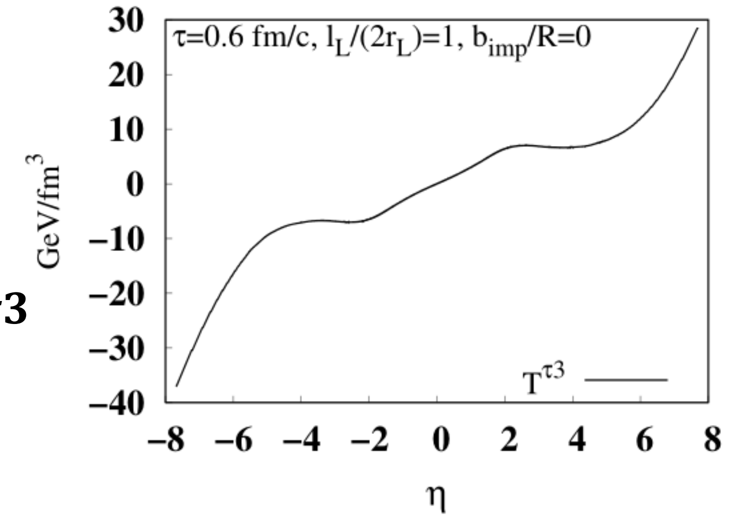

$T^{\tau 3}$

- $T^{\tau 3}$ is found to increase with |η| in the large rapidity region
- CYM fields exist in the large rapidity region and contribute to $T^{\tau 3}$

Assumption

We assume that within the CYM fields, there is a glasma part, which will eventually become QGP, and a non-glasma part, with the majority of the latter consisting of WW fields

Subtraction Method

Focusing on the fact that ε_{LRF} of the WW fields is zero, while that of the glasma is large, we differentiate between the glasma and non-glasma parts in the CYM fields based on the magnitude of ε_{LRF}, and define the EM tensor of the glasma part as

$$\boxed{T^{\mu\nu}_{\mathrm{gl}} = \theta(\varepsilon_{\mathrm{LRF}} - \varepsilon_{\mathrm{c}})T^{\mu\nu}}$$

<u>***$T^{\tau 3}$ with the subtraction method***</u>

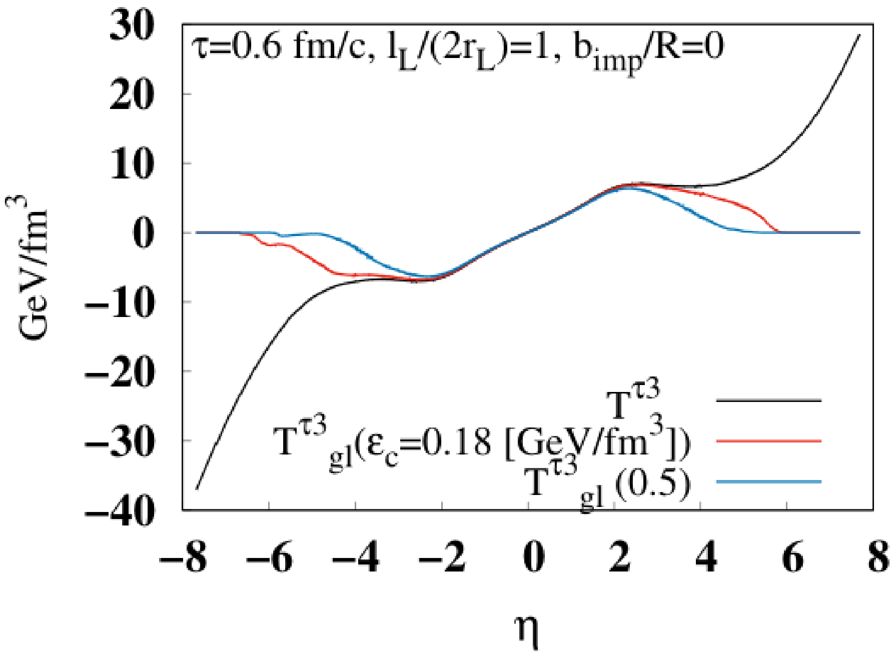

- At |η| < 2, the newly defined $T_{\mathrm{gl}}^{\tau 3}$ agrees well with the original one
- At |η| > 2, in contrast to the original one, $T_{\mathrm{gl}}^{\tau 3}$ goes to zero as the rapidity becomes larger

Rapidity Profile of L at Non-Central Collisions

Rapidity distribution of Angular momentum

$$\frac{dL^2}{d\eta} \equiv \int d^2\boldsymbol{x}_\perp \tau \frac{1}{2}\varepsilon^{2ij} M^\tau{}_{ij}$$
$$= \int d^2\boldsymbol{x}_\perp \tau \left(x^3 T^{\tau 1} - x^1 T^{\tau 3}\right)$$

- To focus glasma's contribution, we use $T^{\tau 3}_{\mathrm{gl}}$ as $T^{\tau 3}$
- We omit the transverse component $T^{\tau 1}$ since it should be tiny compared to the longitudinal component $T^{\tau 3}_{\mathrm{gl}}$ in the early stage.

Rapidity Profile of L at Non-Central Collisions

Rapidity distribution of Angular momentum

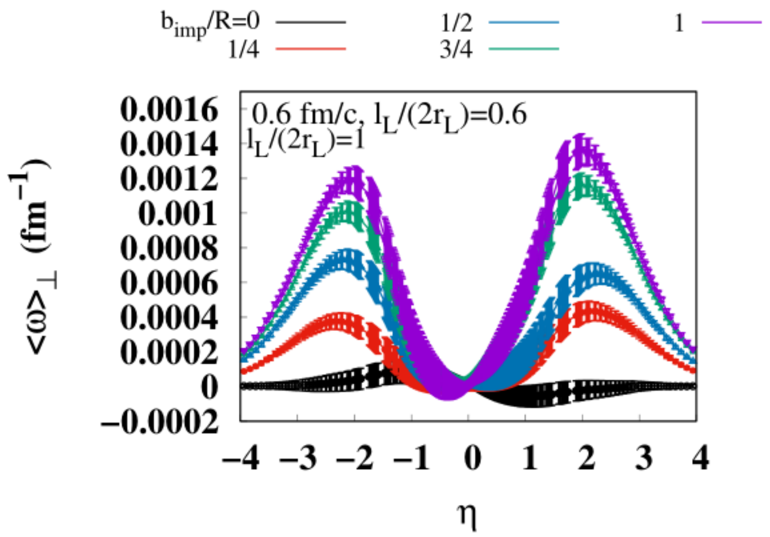

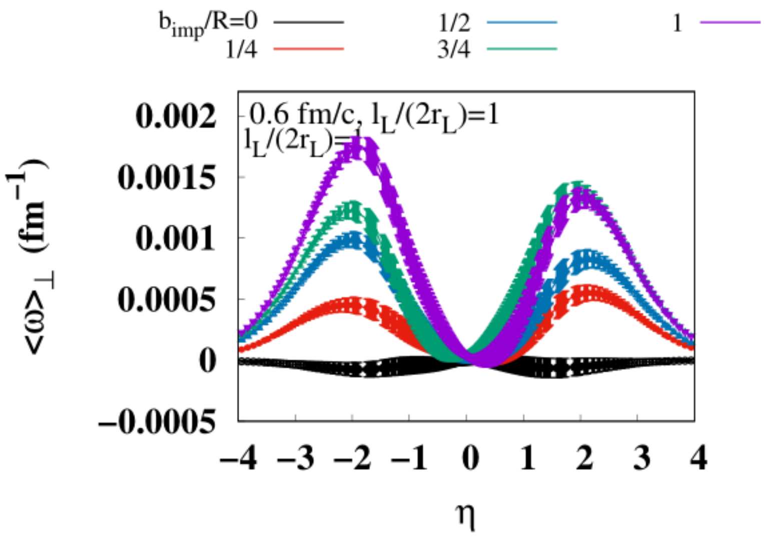

- At $\eta = 0$, the generation of L appears to be zero, regardless of b_{imp}
- As η increases, the generation of L is observed, and its magnitude strongly depends on b_{imp}
- The peak magnitude appears around $\eta = 2 - 3$, which is close to the peak in $T_{\mathrm{gl}}^{\tau 3}$
- The highest peak appears around $\frac{b_{\mathrm{imp}}}{R} = \frac{1}{2} - \frac{3}{4}$, indicating that L depends on b_{imp} non-monotonically

Rapidity Profile of L at Non-Central Collisions

Comment

- Little or no angular L at $\eta = 0$, even for non-zero b_{imp}

- Given that the CGC description is more reliable at higher collision energies, this suggests that little angular momentum would be retained in $\eta = 0$ region in the glasma and subsequently in the QGP at very high energies?

- Effect beyond the high-energy limit's description may be more important for explaining the spin polarization of hadrons observed at mid-rapidity at lower collision energies

Table of Contents

Summary and Outlook

Summary

- We apply the 3D glasma simulation, proposed in our previous work, to the early stage of Au-Au collisions

- We investigate rapidity profiles for a wide range of physical quantities of the glasma in central and non-central collision

Outlook

- The effects not considered in the current calculations, as well as making the model parameters more realistic, should be contemplated to enable more quantitative discussions (ex: $N_c = 2 \rightarrow 3$)
- Additionally, the next step, which is actually being explored currently, is to use the 3D glasma description as an initial state model to provide the initial conditions for hydrodynamics and make comparisons with experimental data.